



This is the accepted manuscript made available via CHORUS, the article has been published as:

Heterobarrier for converting hot-phonon energy to electric potential

Seungha Shin, Corey Melnick, and Massoud Kaviany

Phys. Rev. B **87**, 075317 — Published 19 February 2013

DOI: [10.1103/PhysRevB.87.075317](https://doi.org/10.1103/PhysRevB.87.075317)

Hot phonon as harvestable energy commodity

Seungha Shin, Corey Melnick, and Massoud Kaviani*

Department of Mechanical Engineering,

University of Michigan, Ann Arbor, Michigan 48109, USA

Abstract

We show that hot phonons emitted in energy conversion or resistive processes can be converted to electric potential in heterobarrier structures. Using phonon and electron interaction kinetics and self-consistent ensemble Monte Carlo, we find the favorable conditions for unassisted absorption of hot phonons and design graded heterobarriers for their direct conversion into electric energy. Tandem barriers with nearly optical-phonon height allow for substantial potential gain without current loss. We find that 19% of hot phonons can be harvested with an optimized GaAs/Al_xGa_{1-x}As barrier structure over a range of current and electron densities, thus enhancing the overall energy conversion efficiency and reducing waste heat.

PACS numbers: 63.20.kd, 73.40.Kp, 74.25.Kc, 79.60.Jv

* kaviani@umich.edu, also with Division of Advanced Nuclear Engineering, Pohang University of Science and Technology, Pohang, 790-784 Republic of Korea

I. INTRODUCTION

Various decays, recombination and drags in energy conversions and many resistive processes (e.g., in electronic circuits) emit phonons, hindering energy relaxation and transport in devices [1–3]. Among the phonon modes, energy relaxation through optical-phonon emission is dominant in semiconductors. Emission rate larger than decay can overpopulate the optical modes compared to their equilibrium population, and 'hot phonons' represent this excess occupancy [4]. Examples include high-power electronic devices [5], frustrated-vibration relaxation of chemisorbed molecules [6], lattice electron stoppage of charged fission fragments [7], and nonradiative decay of hot electrons in optoelectric devices [8]. These hot phonons are finally thermalized, converting their energy to waste heat and generating entropy. To improve the efficiency and mitigate heat generation, the thermalized phonons can be recycled by the anti-Stokes cooling (photo-assisted absorption of phonon), resulting in lower device operating temperatures [9, 10]. Photonics including light emitting diodes show enhanced efficiency through thermoelectrically pumped heat [11]. However, utilizing the hot phonons before thermalization is expected to further improve the efficiency. Also, the removal of the excess phonon through this harvesting will lead to improved thermal management and device performance (reducing the phonon friction in electron transport) [12].

In this letter, we propose the unassisted absorption of hot phonons for direct electric potential gain using semiconductor heterobarriers. Barrier structures have been used in thermionics, thermoelectrics and photovoltaics [13–16], and for selective transmission of hot electrons (for thermoelectric performance enhancement) and heat absorption to restore the equilibrium electron distribution. Here, the heterobarrier structure is designed as an embedded structure rather than a stand-alone device, so that we can place the structure near the hot-phonon source for effective pre-thermalization harvesting. This requires kinetics optimization among the phonon absorption and emission (lifetime τ_{p-e}) and up- and down-conversion (τ_{p-p}). The Monte Carlo method is employed to simulate this electron transport and phonon energy conversion in the diffusive regime, showing electric potential gain and phonon energy absorption.

II. ANALYSIS METHODS

A heterobarrier structure composed of GaAs and $\text{Al}_x\text{Ga}_{1-x}\text{As}$ (x or x_{Al} is the Al content) is chosen for this study. Since $\text{Al}_x\text{Ga}_{1-x}\text{As}$ has a larger bandgap than GaAs and the interface has a band edge discontinuity in the conduction ($\Delta E_c = 0.79x_{\text{Al}}$, $x_{\text{Al}} < 0.41$) and valence bands ($\Delta E_v = -0.46x_{\text{Al}}$) depending on x_{Al} (type I), the barrier height φ_b can be controlled with x_{Al} [17, 18]. We consider electrons as the main charge carriers and barriers in the conduction band. Potential barriers can cause an adverse (or reverse) current by reflection or potential change, so large, forward local electric field formed by x_{Al} grading is introduced in the barrier to compensate this adverse effect [14]. Figure 1 shows the spatial distributions of (i) x_{Al} , (ii) electric field, e_e , (iii) product of electric potential and electron charge, $e_c\varphi_e$ (in conduction band edge), and (iv) optical and acoustic phonon temperatures, $T_{p,O}$ and $T_{p,A}$, in the hot-phonon absorbing barrier (HPAB) structure. The electric current density j_e , drift velocity $u_{e,d}$, and electron transition processes involving phonon absorption are also shown.

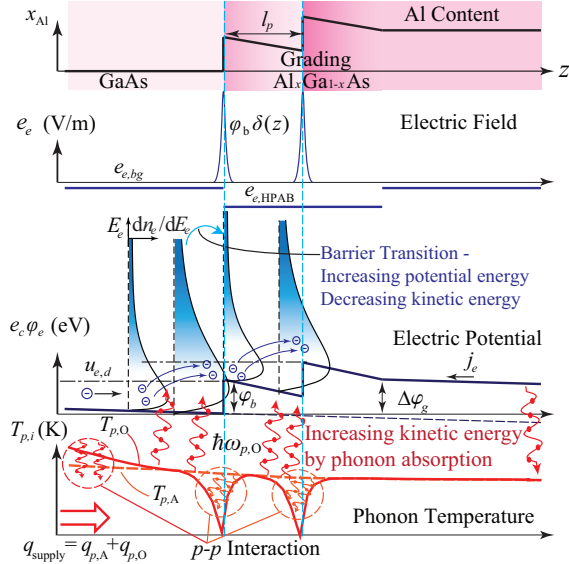


FIG. 1. Spatial distributions of Al content, electric field and potential, and phonon temperatures in the hot-phonon absorbing barrier structure. x_{Al} abruptly increases, creating the potential barrier (with height φ_b) in the conduction band edge, while the grading maintains the current. Phonon absorption populates electrons with higher energy than barrier height ($E_e > \varphi_b$) before or after the barrier transition, and this energy is converted to electric potential. The population of optical phonons quickly decreases at the barriers and recovers by upconversion.

Interaction rates for the kinetics are calculated using the Fermi golden rule (FGR) [19]. Because the single optical phonon interaction with an electron is based on a perturbation by the displacement d , the Hamiltonian with the e - p interaction including the first-order perturbation is expressed as

$$H = H_o + H_{e-p} = (H_{e,o} + H_{p,o}) + \varphi'_{e-p}d, \quad (1)$$

where H_o is the unperturbed Hamiltonian ($H_{e,o} + H_{p,o}$), and H_{e-p} is the interaction Hamiltonian (with the first order e - p coupling φ'_{e-p} , $H_{e-p} = \varphi'_{e-p}d$). Since the displacement $d = [\hbar/(2m\omega_{p,o})]^{1/2}(b^\dagger + b)$, where m is the reduced mass of oscillating atoms, $\omega_{p,o}$ is the phonon frequency, and b^\dagger (b) is the creation (annihilation) operator of phonon, the interaction rate from the FGR is expressed as

$$\dot{\gamma}_{e-p} = \frac{\pi}{m\omega_{p,o}} |\langle \psi_{e,f} | \varphi'_{e-p} | \psi_{e,i} \rangle|^2 |\langle f_p \pm 1 | b^\dagger + b | f_p \rangle|^2 \delta_D(E_{e,f} - E_{e,i} \mp E_{p,o}), \quad (2)$$

where ψ_e is electron wave function, f_p is phonon occupancy, δ_D is the Dirac delta function, and subscripts i and f represent the initial and final states. The interaction matrix element $|\langle \psi_{e,f} | \varphi'_{e-p} | \psi_{e,i} \rangle|^2$ for nonpolar optical phonon is $\phi'^2_{e-p} \delta_{D,\kappa}$, where ϕ'_{e-p} is the deformation potential and $\delta_{D,\kappa}$ is for the momentum conservation ($\kappa_{e,f} = \kappa_{e,i} + \kappa_p$, where κ_e and κ_p are the electron and phonon momentum). For anisotropic polar optical phonon interaction which absorbs or emits longitudinal optical (LO) phonon, the element becomes $(\rho e_c^2 \omega_p^2 / \kappa_p^2)(1/\epsilon_{e,\infty} - 1/\epsilon_{e,s}) \delta_{D,\kappa}$, where $\epsilon_{e,s}$ and $\epsilon_{e,\infty}$ are the static and optical dielectric constants, e_c is the electron charge, and ρ is the density [20]. Since $|\langle f_p \pm 1 | b^\dagger + b | f_p \rangle|^2 = f_p + 0.5 \pm 0.5$, the phonon absorption and emission rates ($\dot{\gamma}_{p \rightarrow e}$ and $\dot{\gamma}_{e \rightarrow p}$) are proportional to f_p and $f_p + 1$, respectively. From δ_D for the energy conservation, the phonon emission occurs only when the initial electron energy is larger than the emitted phonon energy ($E_{e,i} > E_{p,o}$), but the emission rate $\dot{\gamma}_{e \rightarrow p}$ increases with E_e faster than the absorption rate $\dot{\gamma}_{p \rightarrow e}$. With higher φ_b , in order to pass through barriers, electrons require a larger momentum or E_e , or the less energetic electrons need to increase their energy through phonon absorption. However, high-energy carriers are emission-favorable and less populated, and multiphonon absorption for low-energy electron transition is not probable [21]. Thus, tandem-barrier structures with $\varphi_b \leq E_{p,LO} (\approx 35 \text{ meV, only absorption available})$ rather than a single barrier with large height are employed for large potential gain.

The lowest conduction band in GaAs has three valleys, at Γ , L and X, where Γ is heavily populated at room temperature. Electrons in the band are scattered through various mech-

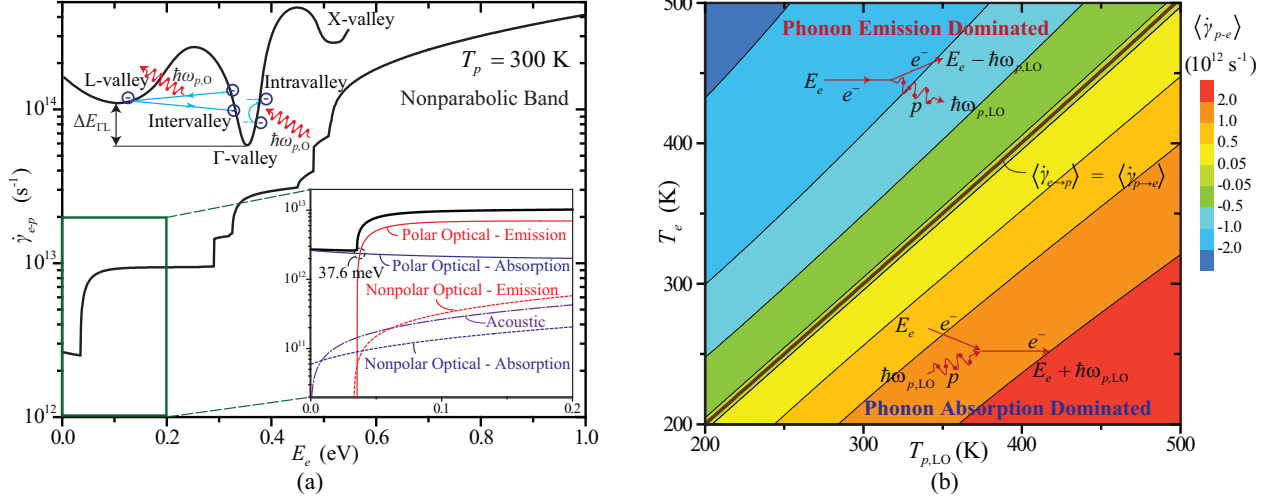


FIG. 2. (a) Variations of the electron interaction rates in the lowest conduction band, as a function of electron energy (E_e) for $T_p = 300$ K. Insets show the band structure and various interaction mechanisms (left) and the interaction rates for low- E_e Γ -valley electrons (right). Polar optical phonon scattering is dominant at low E_e , and intervalley scattering rates increase with E_e . (b) Average polar optical phonon absorption (+)/emission (-) rates as functions of T_e and $T_{p,LO}$. The phonon absorption or emission rate becomes faster as nonequilibrium between electron and phonon increases.

anisms, and the overall interaction rates are shown in Fig. 2(a). The Γ -valley polar optical phonon interaction, which absorbs or emits longitudinal optical (LO) phonon, dominates for low E_e , and intervalley scattering is dominant when $E_e > \Delta E_{\Gamma L}$ (energy difference between Γ - and L-valleys). Average absorption $\langle \dot{\gamma}_{p \rightarrow e} \rangle$ and emission $\langle \dot{\gamma}_{e \rightarrow p} \rangle$ rates for Γ -valley is obtained considering LO phonon temperature $T_{p,LO}$ ($= E_{p,LO} / \{k_B [\ln(f_{p,LO} + 1) - \ln(f_{p,LO})]\}$) and electron distribution dn_e/dE_e ($D_e f_e^o$, where D_e is the density of states and f_e^o is the equilibrium electron distribution), and favorable absorption/emission is also shown in Fig. 2(b).

The rate of three-phonon (p - p) interactions (up- and downconversion), competing with the e - p interactions, are given by [22]

$$\dot{\gamma}_{p-p, \text{down/up}} = \frac{\hbar}{8\pi\rho^3} \frac{|M_{p-p}|^2 R}{u_{p,A}^7 u_{p,O}^2} \omega_{p,A}^2 \omega_{p,O}^3 [f_p(\omega_{p,A}) + 0.5 \pm 0.5]^2 [f_p(\omega_{p,O}) + 0.5 \mp 0.5], \quad (3)$$

where $u_{p,A}$, $u_{p,O}$, $\omega_{p,A}$ and $\omega_{p,O}$ are the acoustic and optical phonon speeds and frequencies, $|M_{p-p}|^2$ is $4\rho^2 \gamma_G^2 u_{p,A}^2 u_{p,O}^2$, ρ is the density, γ_G is the Grüneisen parameter, and R is obtained

from the force constants estimated by material metrics in [23]. (With $\rho_{\text{GaAs}} = 5317 \text{ kg/m}^3$, $u_{p,A} = 2800 \text{ m/s}$, $\gamma_G = 0.8$ and $R = 0.128$, $\dot{\gamma}_{p-p}$ is 4.3 ps at 300 K, which agrees well with experiments [24, 25].) Since the $e-p$ interaction rate is faster than the $p-p$, the electron is first excited and relaxed to equilibrium during the hot-phonon relaxation, and thus within a ps, it has large population at high E_e (desirable for barrier transition). Thus, considering this downconversion of optical phonons along with their low mobility, HPAB placed near the phonon source is suited for harvesting hot phonons.

Self-consistent ensemble Monte Carlo (MC) simulates the electron transport and phonon absorption/emission in HPAB with large ensemble of sampled electrons coupling to the Poisson equation to reflect the internal charge redistribution [26–28]. The simulation includes acoustic, inter- and intravalley optical phonon scatterings in the lowest conduction band, and employs GaAs properties (effective mass $m_{e,e}$, dielectric constants $\epsilon_{e,\infty}$ and $\epsilon_{e,s}$, deformation potential ϕ'_{e-p} , etc.) [20, 29], as the small φ_b requires a small change of x_{Al} and physical properties ($\sim 4\%$ change of x_{Al} per barrier). The predicted electron mobility μ_e agrees well with experiments for bulk GaAs ($\mu_{e,\text{GaAs}} = 0.85 \text{ m}^2/\text{V-s}$ for low e_e and decreases with e_e) for all electric fields [30], verifying the algorithm. Sampled electrons travel with the prescribed electric potential along z as in Fig. 1 (the particle distribution in the lateral directions is not considered). Initially 200,000 electrons over $1 \mu\text{m}$ region are sampled, and various numbers of barriers N_b are placed with barrier pitch l_p in the center. Particles are initially in Γ -valley according to the equilibrium distribution with T_e . An appropriate background electric field $e_{e,bg}$ is applied to create a reference current density $j_{e,o}$ (or drift velocity $u_{e,d,o}$) without barrier, and a higher local electric field $e_{e,\text{HPAB}}$ (from the x_{Al} grading) is applied to the barrier region. The z -direction boundaries are assumed to have constant charge distribution, and electrons are supplied to compensate for those exiting.

To maintain the phonon population (depends on T_p through the Bose-Einstein distribution), phonon flux sufficient for the absorption over the simulation region is prescribed at the left boundary. Phonon transport and distribution are also simulated along with electrons through the phonon conductivity (k_p), $e-p$ interaction rates (for phonon absorption and emission, $\dot{\gamma}_{p \rightarrow e}$ and $\dot{\gamma}_{e \rightarrow p}$), and $p-p$ up- and downconversion rates ($\dot{\gamma}_{p \rightarrow p, \text{up}}$ and $\dot{\gamma}_{p \rightarrow p, \text{down}}$) [31]. Because the hot phonon effect is prominent only in the LO phonon mode [32], the conservation of the LO phonon (dominant in phonon absorption) and all other phonon modes (A) are separately tracked in each bin. Over the spatial increment ($\Delta z = 5 \text{ nm}$), the phonon

energy change (per area) in the j -th bin (z_j) over a time step ($\Delta t, t \sim t + \Delta t$) is

$$\Delta E_{p,i}(z_j) = \Delta t \{ -(q_{p,i,L} + q_{p,i,R}) + [\dot{s}_{e-p,i}(z_j) \pm \dot{s}_{p-p,\text{up}}(z_j)] \Delta z \}, \quad (4)$$

where i is a phonon mode (LO or A, + for LO and - for A), and $q_{p,i,R}$ (or $q_{p,i,L}$) is the phonon flux from the neighboring bins, determined by $T_{p,i}$ and $k_{p,i}$ ($k_{p,A} = 54$ W/K-m and $k_{p,LO} = 1$ W/K-m, approximated from [33]) as

$$q_{p,i,R \text{ or } L} = \frac{k_{p,i}}{\Delta z} [T_{p,i}(z_j) - T_{p,i}(z_j \pm \Delta z)]. \quad (5)$$

$q_{p,i,L}$ at the left boundary is prescribed (q_{supply} is set to total phonon absorption), and $q_{p,i,R}$ on the right is calculated using an external thermal resistance (equivalent to 20 μm of GaAs) and the surrounding temperature (T_o). $\dot{s}_{e-p,i}$ and $\dot{s}_{p-p,\text{up}}$ depend on the electron distribution and phonon temperatures, and are found from MC simulation and Eq. (3). Using $\Delta E_{p,i}$, heat capacity ($c_{p,i}$) [34], and LO phonon energy, the spatial distributions of $T_{p,A}$ and $T_{p,LO}$ are updated.

In barrier transition, electrons lose (forward) or gain (backward) momentum corresponding to φ_b with the nonconserving lateral momentum [15, 35], and tunneling is not considered. With the lateral momentum conservation, smaller barrier transition efficiency is expected. Although epitaxial planar GaAs/AlGaAs heterostructures have shown that lateral momentum is mostly conserved, introducing surface roughness is expected to break the conservation and enhance the barrier transition [35, 36]. The Fermi level, away from the HPAB, has the same distance from the band edge, due to the same level of doping and electron distribution. The potential gain through each barrier structure is estimated as $\Delta\varphi_{g,o} = \varphi_b + e_{e,\text{HPAB}} l_p$ (when the internal field by charge redistribution is not significant), and total potential gain is proportional to the number of barriers ($\Delta\varphi_g = N_b \Delta\varphi_{g,o}$). Note that $\Delta\varphi_g$ increases the required x_{Al} , which changes the properties (increase in the optical phonon energy $E_{p,LO}$ and decrease in the electron mobility μ_e due to larger $m_{e,e}$ and intervally scattering). Our simulation results with GaAs properties can be more safely accepted for lower $\Delta\varphi_g$. Properties from simulations (e.g., electron and phonon distribution, drift velocity, temperatures, and phonon absorption rate) are obtained by the ensemble average of the sampled particles from 0.5 to 1 ns.

III. RESULTS AND DISCUSSIONS

The MC simulations demonstrate that the HPAB produces electric potential gain without current loss through a proper combination of the local barrier electric field ($e_{e,\text{HPAB}}$), the optical phonon population ($f_{p,\text{LO}}$), and the barrier height (φ_b), and the potential energy gain is based on phonon absorption. Since the adverse current caused by the barrier decreases with increasing $f_{p,\text{LO}}$ (or $T_{p,\text{LO}}$) due to large phonon absorption rate [as in Fig. 2(b)], larger $\Delta\varphi_g$ with smaller $e_{e,\text{HPAB}}$ can be achieved at higher $T_{p,\text{LO}}$. However, a large phonon population also increases the scattering rate, thus decreasing μ_e . Acoustic phonons do not contribute to electron upconversion, so low $T_{p,A}$ and high $T_{p,\text{LO}}$ are desirable. With constant $T_{p,A}$ and $T_{p,\text{LO}}$, HPAB operating under high $T_{p,\text{LO}}$ has smaller current loss and larger $\Delta\varphi_g$ compared to the thermal equilibrium system. (Nonequilibrium $T_{p,\text{LO}} = 325$ K and $T_{p,A} = 300$ K in GaAs relaxes to an equilibrium temperature of 304 K from the energy conservation, and $\Delta\varphi_{g,o}$ reduces from 20.03 to 19.57 meV. Barrier transition is more effective in hot phonon

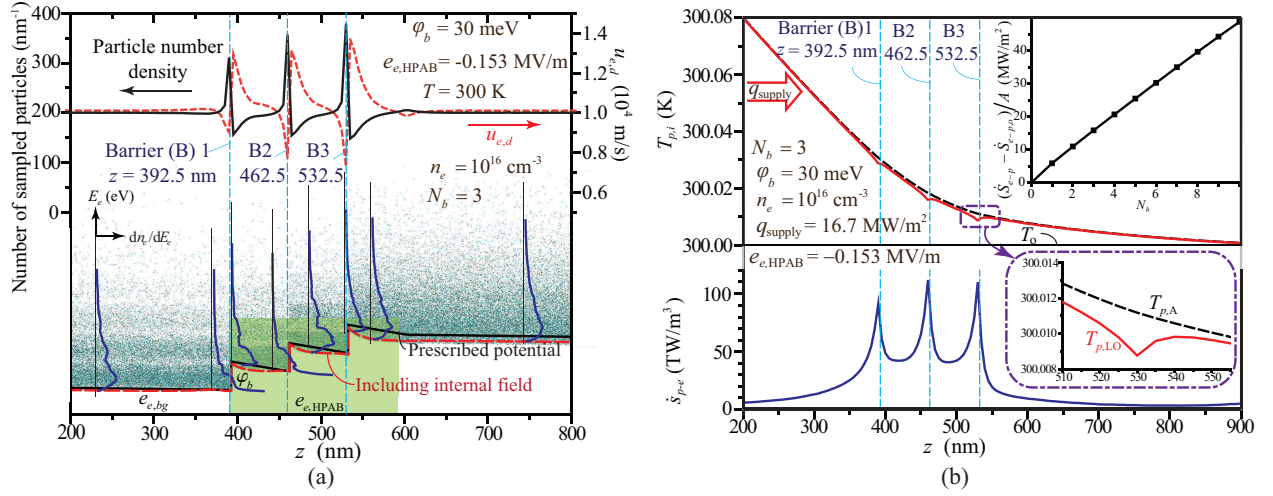


FIG. 3. (a) Sampled particle number density, drift velocity ($u_{e,d}$), and particle-energy distributions over the simulation cell. Electrons are accumulated behind barriers and low-energy electrons are highly populated near barriers. (b) Distributions of phonon temperatures ($T_{p,A}$ and $T_{p,\text{LO}}$) and phonon energy absorption rate (\dot{s}_{p-e}). Large phonon absorption occurs around the barriers because of the large population of low-energy electrons, and this leads to the extended nonequilibrium between phonon modes. The total phonon absorption rate in HPAB (\dot{S}_{p-e}/A) is proportional to the number of barriers, as in the inset (top-right).

systems [32].)

The particle density and velocity distributions in Fig. 3(a) show the electron accumulation and the low electron velocity behind the barriers. As Fig. 3(a) also shows, the potential profile near the barriers is bent by this nonuniform charge distribution, and this effect is not significant for small n_e ($< 10^{17}$ cm $^{-3}$). While the electron energy distribution dn_e/dE_e without a barrier is consistent and close to equilibrium, the low-energy electron density is large in the proximity of the barriers because of low transmission and energy loss by barrier. The phonon energy absorption rate ($\dot{s}_{p-e} = \dot{S}_{p-e}/V$, W/m 3) is determined by the electron energy distribution (dn_e/dE_e), i.e.,

$$\dot{s}_{p-e} = \sum_j \int_{E_e} [\dot{\gamma}_{p \rightarrow e, j}(E_e) - \dot{\gamma}_{e \rightarrow p, j}(E_e)] E_{p, j} \frac{dn_e(E_e)}{dE_e} dE_e, \quad (6)$$

where j is an interaction mechanism. Because of the large population at low E_e and no phonon emission with $E_e < E_{p, j}$, the large \dot{s}_{p-e} is observed near the barriers as in Fig. 3(b).

As shown in Fig. 3(b), the variation of $T_{p, i}$ in simulation region (< 1 μ m) is rather small (< 1 K), unless $q_{p, i}$ is extremely large (> 55 MW/m 2), but a rather large difference between $T_{p, LO}$ and $T_{p, A}$ appears near the barriers due to the large \dot{s}_{p-e} . However, since the phonon density ($n_{p, LO} = f_{p, LO}/V_{prim} = 7.56 \times 10^{21}$ cm $^{-3}$ at 300 K, V_{prim} is the primitive cell volume) is more than the four order-of-magnitude larger than n_e ($< 10^{17}$ cm $^{-3}$), the depletion of LO phonons is not significant and is quickly made up by upconversion of acoustic phonons (in spite of smaller $\dot{\gamma}_{p-p}$ than $\dot{\gamma}_{e-p}$). As phonons are absorbed, q_p (gradient of T_p) decreases with z , and vanishes when q_{supply} is completely absorbed. This also shows that hot phonons do not propagate due to the fast relaxation, and therefore, HPAB should be near the hot phonon generation site for high absorption efficiency.

The distribution recovers to equilibrium within a short distance from the barrier (by populating high-energy electrons due to large phonon absorption as well as field acceleration). Unless the electron distribution recovers its population over φ_b before the next barrier, large adverse current is induced by this ineffective barrier transition, and therefore, HPAB should have sufficiently large l_p to enable recovery. However, a long l_p leads to larger potential loss through $e_{e, HPAB}$, and needs to be optimized. Phonon absorption must occur at least once to recover the energy loss ($\leq E_{p, LO}$), so the required distance can be approximated as $l_p = u_{e, z} \tau_{p \rightarrow e, LO}$, where $u_{e, z}$ is the electron velocity in the z direction and $\tau_{p \rightarrow e, LO}$ is the time constant of LO phonon absorption ($1/\dot{\gamma}_{p \rightarrow e, LO}$), and this increases with φ_b . Considering an

average $u_{e,z} = 1.5 \times 10^5$ m/s (from the isotropic velocity distribution) and $\tau_{p \rightarrow e, LO} = 0.4$ ps for equilibrium electrons moving with the forward direction below $E_{p, LO}$, we estimate $l_p = 60$ nm for LO phonon absorption and we choose $l_p = 70$ nm for this work. The MC results also demonstrate that the adverse current by two barriers is almost saturated with $l_p \geq 70$ nm and $\varphi_b \leq E_{p, LO}$.

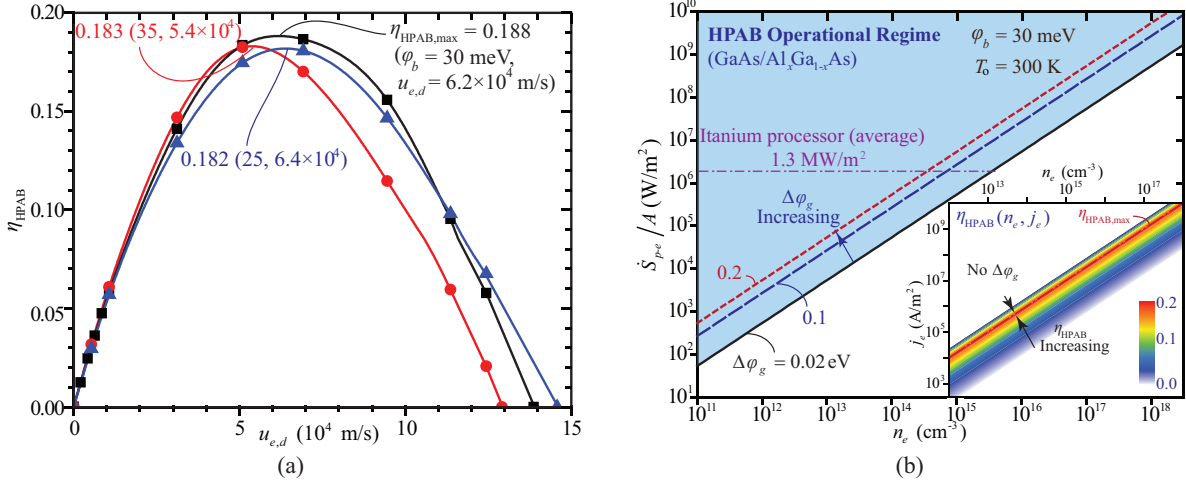


FIG. 4. (a) Variations of the HPAB efficiency (η_{HPAB}) with respect to the drift velocity ($u_{e,d}$). η_{HPAB} first increases with $u_{e,d}$ due to increase in the electrical power gain ($P_g = \Delta\varphi_g j_e$) and then decreases because of smaller $\Delta\varphi_g$. The maximum efficiency $\eta_{HPAB, max}$ is 18.8% for $u_{e,d} = 6.2 \times 10^4$ m/s and $\varphi_b = 30$ meV. (b) HPAB operational regime and variations of phonon energy absorption rate \dot{S}_{p-e}/A with respect to n_e , for $\Delta\varphi_g = 0.02, 0.1,$ and 0.2 eV, and $u_{e,d} < 10^4$ m/s. Inset shows variations of η_{HPAB} with respect to n_e and j_e . \dot{S}_{p-e}/A (for $\Delta\varphi_g$ and j_e corresponding to $\eta_{HPAB, max}$) increases with n_e .

The total phonon absorption rate for the HPAB operation (\dot{S}_{p-e}/A , W/m²) is the integration of \dot{s}_{p-e} over the simulation region, and is almost proportional to n_e (more electrons absorbing more phonons), especially when n_e is low (because of small effect of the charge redistribution). Also, \dot{S}_{p-e}/A increases with N_b or $\Delta\varphi_g$ due to increase in the transitions (linear proportionality for more than two barriers). So, \dot{S}_{p-e}/A can be expressed as $a_{p-e} n_e \Delta\varphi_g$ by introducing the parameter a_{p-e} (A/m). The phonon boost to electrical power per unit area (without current loss) is $P_g = \Delta\varphi_g j_e$. Electrical energy balance in HPAB is

$$\dot{S}_{p-e}/A - q_e = P_g [= N_b(\varphi_b + e_{e, HPAB} l_p) n_e e_c u_{e,d}], \quad (7)$$

where q_e is the kinetic energy flux of egressing electrons. Thus, the HPAB efficiency is the ratio of the power gain (electric potential) and the absorbed phonon energy rate,

$$\eta_{\text{HPAB}} = \frac{P_g}{\dot{S}_{p-e}/A} = \frac{e_c u_{e,d}}{a_{p-e}} \quad (\text{using } P_g = \Delta\varphi_g e_c n_e u_{e,d} \text{ and } \dot{S}_{p-e}/A = a_{p-e} n_e \Delta\varphi_g). \quad (8)$$

Higher $u_{e,d}$ yields larger P_g , but it also leads to larger potential drop from the increased electric field ($u_{e,d}$ larger than 1.38×10^5 m/s cannot gain potential with $\varphi_b = 30$ meV), and thus a_{p-e} increases with $u_{e,d}$ (because of smaller $\Delta\varphi_g$). Since the increase in a_{p-e} becomes more pronounced with higher $u_{e,d}$, η_{HPAB} has a maximum ($\eta_{\text{HPAB,max}}$). \dot{S}_{p-e}/A and $\Delta\varphi_g$ also depend on φ_b because higher φ_b requires larger $e_{e,\text{HPAB}}$ and more phonon absorption per barrier. The simulation results for various $u_{e,d}$ and φ_b show that $\eta_{\text{HPAB,max}}$ is 18.8% when $u_{e,d} = 6.2 \times 10^4$ m/s and $\varphi_b = 30$ meV, as presented in Fig. 4(a). The phonons are provided by an external source, so higher η_{HPAB} is expected by including the phonons emitted in HPAB.

HPAB requires sufficient phonon supply, otherwise phonon depletion reduces $T_{p,\text{LO}}$ and the adverse current increases, which in turn results in charge redistribution diminishing the potential gain. The required phonon energy for low $u_{e,d}$ ($< 10^4$ m/s) and various n_e and $\Delta\varphi_g$ is estimated by extrapolation from the simulations of low n_e ($= 10^{11}$ cm $^{-3}$) with $\varphi_b = 30$ meV and is shown Fig. 4(b). In order for HPAB to operate in a system with larger n_e or $\Delta\varphi_g$, more \dot{S}_{p-e}/A should be provided. The j_e required for high η_{HPAB} is selected depending on n_e due to the dominant dependence of η_{HPAB} on $u_{e,d}$. (j_e for $\eta_{\text{HPAB,max}}$ also increases with n_e .) In the conventional electron density ranges (10^{16} to 10^{18} cm $^{-3}$), large \dot{S}_{p-e}/A ($> 10^6$ W/m 2) and j_e (10^6 to 10^{10} A/m 2) are necessary for high η_{HPAB} , and heat dissipation from some state-of-the-art integrated processors is in this range [37]. Since HPAB is placed close to phonon source, this is local value at a site (e.g. drain-source channel in high-mobility electron transistors) [38, 39].

IV. CONCLUSIONS

In conclusion, we propose the heterobarrier structure for the direct energy conversion from phonon energy to electric potential. This HPAB combines an abrupt barrier with a gradual potential decrease which creates favorable condition for unassisted phonon absorption by increasing the low-energy electron population. The absorbed phonon energy turns into

harvestable electric potential without current loss. The HPAB reverses the phonon role, which generally hinders electron transport, by harvesting hot phonons which would otherwise turn into waste heat.

Through MC simulations, we estimate up to 19% of the phonon energy conversion with proper phonon flux and current. The theoretical efficiency of the HPAB can be estimated by the entropy study, and will be discussed in a separate communication. In addition to gaining electric potential (or recovery), integrating HPAB in electronic devices will reduce heat dissipation, lowering operation temperature and enhancing the electron transport (higher mobility) through the effective removal of excess phonons as a heat sink.

ACKNOWLEDGMENTS

This work is supported by the Center for Solar and Thermal Energy Conversion at University of Michigan, an Energy Frontier Research Center funded by the US Department of Energy, Office of Science, Office of Basic Energy Sciences under Award Number DE-SC0000957. Fruitful discussions with Jamie Phillips, Tomas Palacios, Jedo Kim and Taehwa Lee are greatly appreciated.

-
- [1] J. N. Fehr, M.-A. Dupertuis, T. P. Hessler, L. Kappei, D. Marti, F. Salleras, M. S. Nomura, B. Deveaud, J.-Y. Emery, and B. Dagens, *IEEE J. Quantum Elect.* **38**, 674 (2002).
 - [2] B. K. Ridley, W. J. Schaff, and L. F. Eastman, *J. Appl. Phys.* **96**, 1499 (2004).
 - [3] K. T. Tsen, R. P. Joshi, D. K. Ferry, A. Botchkarev, B. Sverdlov, A. Salvador, and H. Morkoç, *Appl. Phys. Lett.* **68**, 2990 (1996).
 - [4] P. Kocevar, *Physica B* **134**, 155 (1985).
 - [5] A. Matulionis, J. Liberis, I. Matulionien, H. Y. Cha, L. F. Eastman, and M. G. Spencer, *J. Appl. Phys.* **96**, 6439 (2004).
 - [6] S. Sakong, P. Kratzer, X. Han, K. Laß, O. Weingart, and E. Hasselbrink, *J. Chem. Phys.* **129**, 174702 (2008).
 - [7] A. Goland and A. Paskin, *J. Appl. Phys.* **35**, 2188 (1964).

- [8] G. Conibeer, R. Patterson, L. Huang, J.-F. Guillemoles, D. König a, S. Shrestha, and M. Green, *Sol. Energ. Mat. Sol. Cells* **94**, 1516 (2010).
- [9] X. Ruan and M. Kaviani, *ASME J. Heat Transfer* **129**, 3 (2007).
- [10] J. Kim and M. Kaviani, *Appl. Phys. Lett.* **95**, 074103 (2009).
- [11] P. Santhanam, D. J. Gray, and R. J. Ram, *Phys. Rev. Lett.* **108**, 097403 (2012).
- [12] A. Matulionis, *Phys. Stat. Sol. (a)* **203**, 2313 (2006).
- [13] A. Shakouri and J. Bowers, *Appl. Phys. Lett.* **71**, 1234 (1997).
- [14] A. Shakouri, E. Lee, D. Smith, V. Narayanamurti, and J. Bowers, *Microscale Thermophys. Eng.* **2**, 37 (1998).
- [15] R. Kim, C. Jeong, and M. Lundstrom, *J. Appl. Phys.* **107**, 054502 (2010).
- [16] F. Ragay, E. Ruigrok, and J. Wolter, *IEEE WCPEC.* **2**, 1934 (1994).
- [17] Q. S. Zhu, S. M. Mou, X. C. Zhou, and Z. T. Zhong, *Appl. Phys. Lett.* **62**, 2813 (1993).
- [18] M. E. Levinshtein, S. L. Rumyantsev, and M. Shur, *Handbook Series on Semiconductor Parameters* (World Scientific, London, 1996).
- [19] M. Kaviani, *Heat Transfer Physics* (Cambridge University Press, Cambridge, 2008).
- [20] M. Lundstrom, *Fundamentals of Carrier Transport* (Cambridge, 2000).
- [21] S. Egorov and J. Skinner, *J. Chem. Phys.* **103**, 1533 (1995).
- [22] G. P. Srivastava, *The Physics of Phonons* (Adam Hilger, Bristol, 1990).
- [23] B. L. Huang and M. Kaviani, *J. Appl. Physics* **100**, 123507 (2006).
- [24] W. Cai, M. C. Marchetti, and M. Lax, *Phys. Rev. B* **35**, 1369 (1987).
- [25] V. Spagnolo, G. Scamarcio, M. Troccoli, F. Capasso, C. Gmachl, A. M. Sergent, A. L. Hutchinson, D. L. Sivco, and A. Y. Cho, *Appl. Phys. Lett.* **80**, 4303 (2002).
- [26] K. Hess, *Monte Carlo Device Simulation: Full Band and Beyond* (Kluwer Academic Publishers, 1991).
- [27] C. Jacoboni and P. Lugli, *The Monte Carlo Method for Semiconductor Device Simulation* (Springer-Verlag, 1989).
- [28] C. Moglestue, *Monte Carlo Simulation for Semiconductor Device* (Chapman and Hall, 1993).
- [29] A. Dargys and J. Kundrotas, *Handbook on Physical Properties of Ge, Si, GaAs and InP* (Science and Encyclopedia Publishers, 1994).
- [30] J. Ruch and G. Kino, *Phys. Rev.* **174**, 921 (1968).
- [31] M. Zebarjadi, A. Shakouri, and K. Esfarjani, *Phys. Rev. B* **74**, 195331 (2006).

- [32] K. Kim, K. Hess, and F. Capasso, *Appl. Phys. Lett.* **52**, 1167 (1988).
- [33] T. Luo, J. Garg, J. Shiomi, K. Esfarjani, and G. Chen, *Europhys. Lett.* **101**, 16001 (2013).
- [34] S. Tiwari, *Compound Semiconductor Device Physics* (Academic Press, 1992).
- [35] D. Vashaee and A. Shakouri, *Phys. Rev. Lett.* **92**, 106103 (2004).
- [36] Z. Bian and A. Shakouri, *Appl. Phys. Lett.* **88**, 012102 (2006).
- [37] F. J. Pollack, in *32nd IEEE Annual International Symposium on Microarchitecture* (1999).
- [38] W. Saito, Y. Takada, M. Kuraguchi, K. Tsuda, I. Omura, T. Ogura, and H. Ohashi, *IEEE T Electron Dev.* **50**, 2528 (2003).
- [39] T. Palacios, A. Chakraborty, S. Heikman, S. Keller, S. P. DenBaars, and U. K. Mishra, *IEEE Electr. Device L.* **27**, 13 (2006).